

DTC Versus Vector Control Strategies for a Grid Connected DFIG-Based Wind Turbine



Khaled Kouider and Abdelkader Bekri

Abstract With the high level of wind power penetration, system executives have an increasing interest in investigating the wind power integration influence on power systems. The doubly fed induction generator (DFIG) is commonly employed in wind power generation systems. In this chapter, we focus on the direct torque and the classic vector control applied to the rotor side converter (RSC) of a grid-connected doubly fed induction generator (DFIG) using a detailed dynamic model under dq reference frame. The two strategies are compared considering many parameters as the rotor currents, the stator power, electromagnetic torque, and rotor flux to ensure the proper operation and to enhance the performance of the DFIG. Both control strategies of our machine are simulated using MATLAB/SIMULINK software package. Finally, the simulations results are displayed and well discussed.

Keywords Direct torque control · Hysteresis · Lock-up table · Vector control · Stator flux orientation

1 Introduction

Nowadays, the electrical power consumption increases proportionally with the human society. It is reported by Enerdata [1], that the global net electricity consumption has risen from 21,463 TWh in 2016 to 22,015 TWh in 2017 (the power consumption accelerated again in 2017 (+2.3%)). Since the major part of electricity is generated from fossil fuels, the increase in net electricity consumption will result in significant greenhouse gas emissions, which could lead to global warming [2]. For this reason, the renewable energies occupied a crucial position in the last research. The wind power generation is regarded as the most widely used non-hydro renewable energy generation with a renewable and clean high reserve. Besides, it provides almost no greenhouse gas emissions [2]. In the same context,

K. Kouider (✉) · A. Bekri

Department of Electrical Engineering, University of Tahri Mohammed, Bechar, Algeria

© Springer Nature Switzerland AG 2022

M. Elhoseny et al. (eds.), *Distributed Sensing and Intelligent Systems*, Studies in Distributed Intelligence, https://doi.org/10.1007/978-3-030-64258-7_62

723

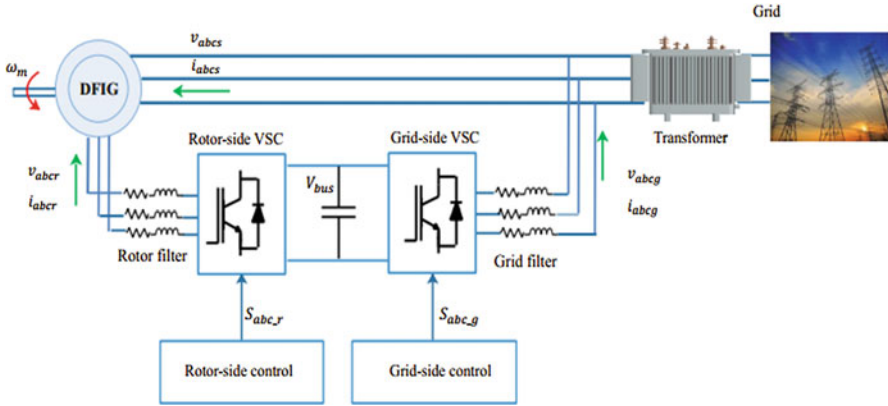


Fig. 1 A standard configuration of a doubly fed induction generator (DFIG) wind power system

and due to many technical and economic factors like the partial scale converting using an economical converter size to handle a fraction (20–30%) of the total power, the doubly fed induction generator (DFIG)-based wind turbine is considered one of the most practical solutions for the wind power conversion. A regular arrangement of a DFIG-WT system is illustrated in Fig. 1. A wound rotor induction generator with slip ring is essential to conduct current toward or out of the rotor winding at slip frequency.

The variable-speed operation is achieved with the help of injecting a controllable rotor voltage [3]. The DFIG could be operated under three modes: subsynchronous operation when $\omega_m < \omega_s$, hypersynchronous operation while $\omega_m > \omega_s$, and in synchronous mode if $\omega_m = \omega_s$, where ω_s and ω_m are the synchronous rotor electrical speeds allowing a bidirectional power flow from or into the back-to-back converter. The grid connection of the DFIG-WT receives a big intention in the last decade. Many works are fulfilled such as the classic vector control as in Dehong et al. [2], Fox et al. [3], Kerrouche et al. [4] and Fei et al. [5] to enhance the performance of the DFIG wind power systems. In the recent years, the direct control techniques have gained a huge importance as in Arnalte et al. [6], and a new improved direct torque control strategy is developed in Li et al. [7]. An ANFIS-based DTC for a DFIG is applied in Kumar et al. [8]. In this chapter, we concentrate on the comparison between the direct torque control and the classic vector control methods for a DFIG wind system. For this purpose, this chapter will be split into three subsections: firstly, the detailed DFIG-WT mathematical model is achieved, then the description of the two control methods laws and equations are established. Finally, the simulation and results are well explained. In this context, this chapter reveals that it is possible to compare the performance of both strategies using various parameters.

2 DFIG in Wind Energy Systems

In this section, the most essential electric and mechanic equations of the DFIG wind system are used to achieve an analytical model proper for the control of the machine. The mathematical modeling of the system is well shown in the two following subsections.

2.1 DFIG Mathematical Modeling

The dynamic model of the DFIG under dq reference frame can be reached using the stator and rotor windings equations as follows [9–11], where ψ_{sd} , ψ_{sq} , ψ_{rd} , ψ_{rq} , i_{sd} , i_{sq} , i_{rd} , i_{rq} are the stator and rotor flux and currents under dq components, respectively, and R_s , R_r , ω_s , ω_r , p are the stator and rotor resistances, speeds, and the number of poles pairs:

$$\begin{aligned} u_{sd} &= R_s i_{sd} + \frac{d\psi_{sd}}{dt} - \omega_s \psi_{sq} \\ u_{sq} &= R_s i_{sq} + \frac{d\psi_{sq}}{dt} + \omega_s \psi_{sd} \\ u_{rd} &= R_r i_{rd} + \frac{d\psi_{rd}}{dt} - \omega_r \psi_{rq} \\ u_{rq} &= R_r i_{rq} + \frac{d\psi_{rq}}{dt} + \omega_r \psi_{rd} \end{aligned} \quad (1)$$

After that the rotor and stator fluxes are given by Eq. (2), where L_s , L_r , L_m are the stator, rotor, and mutual inductances:

$$\begin{aligned} \psi_{sd} &= L_s i_{sd} + L_m i_{rd} \\ \psi_{sq} &= L_s i_{sq} + L_m i_{rq} \\ \psi_{rd} &= L_r i_{rd} + L_m i_{sd} \\ \psi_{rq} &= L_r i_{rq} + L_m i_{sq} \end{aligned} \quad (2)$$

And the electromagnetic torque:

$$T_{em} = \frac{3}{2} p (i_{rd} i_{sq} + i_{rq} i_{sd}) \quad (3)$$

2.2 Aerodynamic Turbine Modeling

The mechanical power P_m received from the wind can be denoted by the complex algebraic equation in function of blade pitch angle β , the rotor blades diameter R , the air density ρ , shaft and wind speed Ω_t , V_w , the tip speed ratio λ , and the power coefficient C_p as shown in Eq. (4):

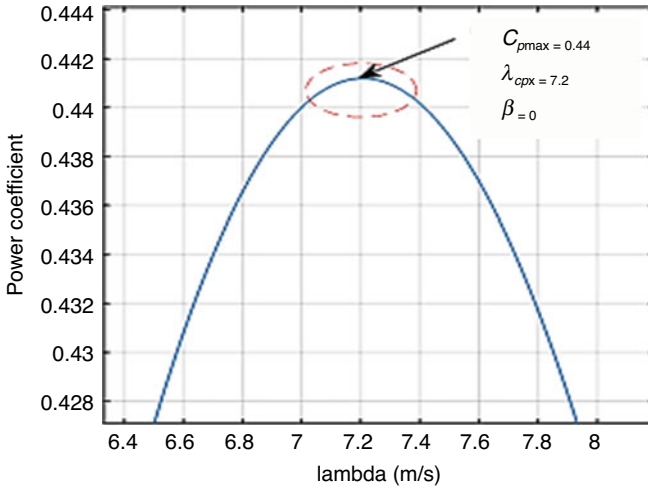


Fig. 2 The power coefficient C_p versus the tip speed ratio λ

$$P_m = \frac{1}{2} \rho \pi R^2 V_w^3 C_p(\lambda, \beta) \tag{4}$$

where λ is the tip speed ratio

$$\lambda = \frac{R \Omega_t}{V_w} \tag{5}$$

In this chapter, we use $C_{p \max} = 0.44$ and $\lambda_{opt} = 7.2$.

The gearbox is an essential part of the wind turbine systems (Fig. 2). It is usually used to adapt the low rotor shaft speed Ω_t to the high speed of the generator Ω_m . The following equations describe it in addition to the mechanical speed evolution:

$$\begin{cases} T_m = \frac{T_{aer}}{G} \\ \Omega_t = \frac{\Omega_m}{G} \end{cases} \tag{6}$$

$$J \frac{d\Omega_m}{dt} = T_m - T_{em} - f \Omega_m \tag{7}$$

3 Control Techniques of the DFIG

As mentioned before, the control strategies used in this chapter are the classic vector control and the direct torque control. Both approaches will be well described in the succeeding two subsections.

3.1 Classic Vector Control

Numerous control approaches are applied for the DFIG control; despite of that the vector control techniques were the most established ones. The use of the dq synchronous reference frame is ordinarily shared between the DFIG and the other machines [12]. From the previous dynamic model of the DFIG, and basing on the d-axis alignment of the stator flux ($\psi_{qs} = 0$), we obtain the two rotor voltage equations:

$$u_{rd} = R_r i_{rd} + \sigma L_r \frac{di_{rd}}{dt} - \omega_r L_r i_{rq} + \frac{L_m}{L_s} \frac{d}{dt} |\vec{\psi}_s| \quad (8)$$

$$u_{rq} = R_r i_{rq} + \sigma L_r \frac{di_{rq}}{dt} - \omega_r L_r i_{rd} + \omega_r \frac{L_m}{L_s} \frac{d}{dt} |\vec{\psi}_s| \quad (9)$$

where σ is the Blondel's coefficient, $\sigma = 1 - \frac{L_m^2}{L_r L_s}$.

Basing on the d -axis alignment as shown in Fig. 3, we see that the reactive power Q_s is directly affected by the current I_{dr} , while the current I_{qr} modified the torque/active power [10] as shown in Eqs. (10) and (11):

$$T_{em} = \frac{3}{2} p (\psi_{qs} i_{dr} - \psi_{ds} i_{qr}) \Rightarrow T_{em} = -\frac{3}{2} p \frac{L_m}{L_s} |\vec{\psi}_s| i_{qr} \quad (10)$$

$$Q_s = -\frac{3}{2} \omega_s \frac{L_m}{L_s} |\vec{\psi}_s| \left(i_{dr} - \frac{|\vec{\psi}_s|}{L_m} \right) \quad (11)$$

The detailed explanations of the vector control technique and the current control loops used in this strategy are well established in [10]. Furthermore, the complete vector control schema used in this chapter is well drawn in Fig. 4.

Fig. 3 Stator flux-oriented in the dq reference frame

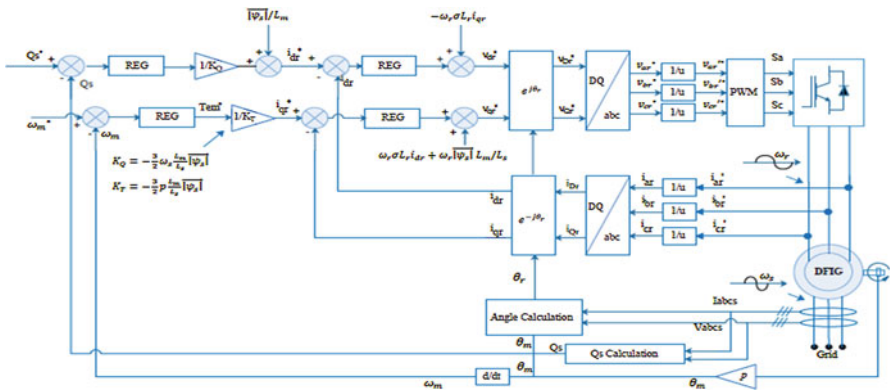
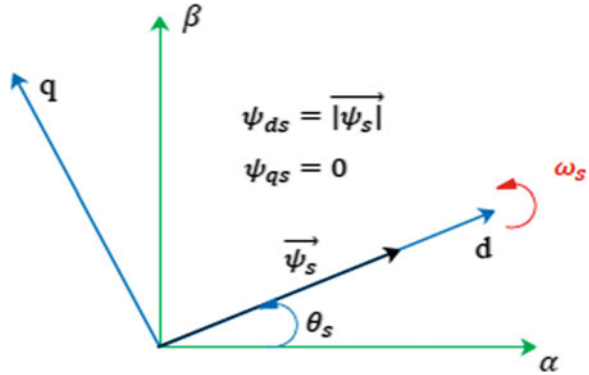


Fig. 4 The overall vector control diagram applied to the rotor side converter (RSC) of the DFIG

3.2 Direct Torque Control Principles for the DFIG

The direct control strategies are recognized like the modern solutions for the AC drives. Usually, from the side of the performance and global features, and compared to the vector control strategies, there are many differences. Several works have fulfilled in this area in Gonzalo et al. [9], Zhang et al. [13], Jihène et al. [14] and Xiong et al. [15], and as a consequence, various contributions to these new techniques are tested for a proper DFIG-based wind turbine applications. Referring to Haitham et al. [10], many facts about the DTC principle can be extracted: first, two variables of the DFIG have immediately commanded: the amplitudes of both rotor flux and the electromagnetic torque. Moreover, the angle δ denotes the distance between both stator and rotor flux vectors and by adjusting this angle we can control the torque. Furthermore, with the help of the injection of different voltage vectors to the rotor of the DFIG, the rotor flux trajectory and amplitude can be directly modified using a two-level voltage source converter (VSC). Eventually, the DTC is nearly related to the VSC that is manipulated. Therefore, the pulses are generated directly without any modulation schema.

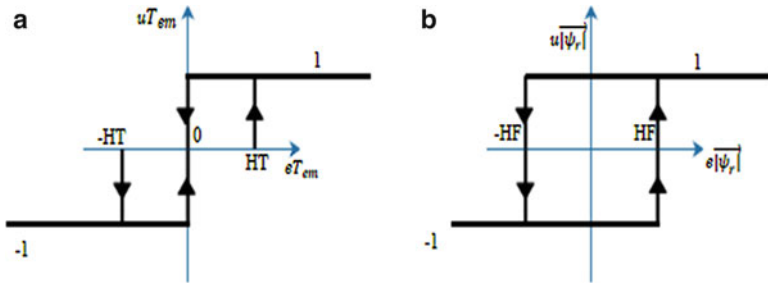


Fig. 5 (a) Three-level hysteresis comparator for the torque, (b) two-level hysteresis comparator for the rotor flux

Two hysteresis comparators are used in the classic DTC; one for the flux controller and it is based on two-level hysteresis comparator with the band HF and the other is based on three-level hysteresis comparator HT for the electromagnetic torque. Practically, the band values are usually restricted using the lowest switching sample time of the implementation tools [16]. Figure 5 shows the two hysteresis controllers for both flux and torque.

After recognizing the fundamental principle of the DTC, the next step is to estimate the main variables of the control technique (T_{em} , rotor flux and the rotor flux angle), which can be described directly by the following equations:

$$T_{em} = \frac{3}{2} p \frac{L_m}{\sigma L_r L_s} |\vec{\psi}_r| |\vec{\psi}_s| \sin \delta \tag{12}$$

$$\psi_{rd} = \int_0^t (V_{rd} - R_r I_{rd})$$

$$\psi_{rq} = \int_0^t (V_{rq} - R_r I_{rq}) \tag{13}$$

$$|\vec{\psi}_r| = \sqrt{\psi_{rd}^2 + \psi_{rq}^2} \tag{14}$$

Besides, after the computation of the rotor flux dq components, it is necessary to determine the rotor flux angle θ_{ψ_r} , then the sectors can be simply calculated.

$$\theta_{\psi_r} = a \tan \left(\frac{\psi_{rq}}{\psi_{rd}} \right) \tag{15}$$

Table 1 Rotor voltage vector selection according to torque and flux errors

		uT_{em}		
		1	0	-1
$u \psi_r $	1		$V_{(i-1)}V_0, V_7V_{(i+1)}$	
	0		$V_{(i-1)}V_0, V_7V_{(i+1)}$	

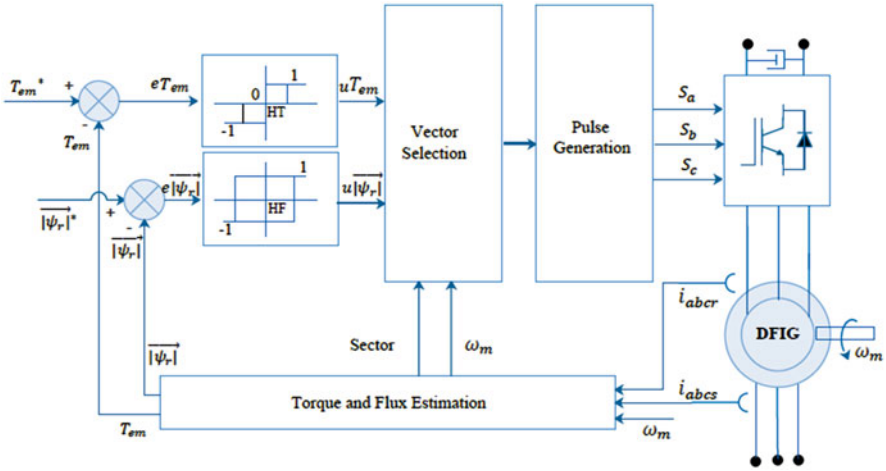


Fig. 6 DTC diagram applied to the RSC of the DFIG

The eight space voltage vectors are calculated using:

$$\begin{cases} V_i = \frac{2}{3} V_{dc} e^{-j\frac{\pi}{3}(i-1)} \\ V_0 = V_7 = 0 \end{cases} \tag{16}$$

where i is the sector number where $i = [1 \dots 6]$.

Then, the selection of the proper rotor space vector is done based on Table 1.

Finally, the entire diagram of the DTC for DFIG wind system is well depicted in Fig. 6.

4 Simulation and Results

The simulation is made using the MATLAB/SIMULINK software package to examine the DTC and vector control strategies performance for a 2 MW DFIG-WT described in the Appendix. In this chapter, two control strategies (DTC and the classic vector control) will be compared to discuss the performance of a 2 MW DFIG-WT. Four parameters will be investigated (the electromagnetic torque T_{em} , the rotor flux ψ_r , the rotor current I_r , the stator power P_s). For the simulation of

both control strategies, we use the magnetization through the stator ($I_{dr} = 0$), and all the parameters used in this simulation are well cited in the Appendix.

4.1 Vector Control Simulation

Figures 7, 8, 9 and 10 show the essential rotor side converter (RSC) variables (rotor currents, rotor flux, the electromagnetic torque, and the stator power). From Fig. 7a, b, we see that the direct and the quadratic components of the rotor currents follow the references after nearly 3 s after a transient.

The rotor flux amplitude and the electromagnetic torque are shown by the Fig. 8a, b; after the transient state, the two variables remain stable state after nearly 5 s and the electromagnetic torque coincide with the reference at that time.

Furthermore, the power delivered by the stator is well illustrated in the Fig. 9, we see that the power after the starting state increased until achieving 1.77 MW at permanent.

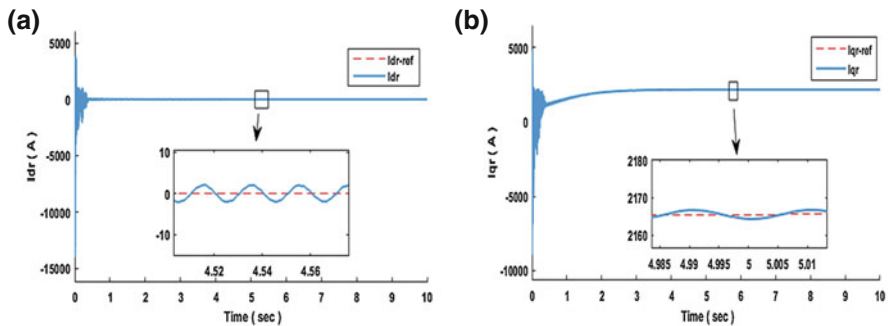


Fig. 7 Dq rotor current components versus references, (a) direct component, (b) quadratic component

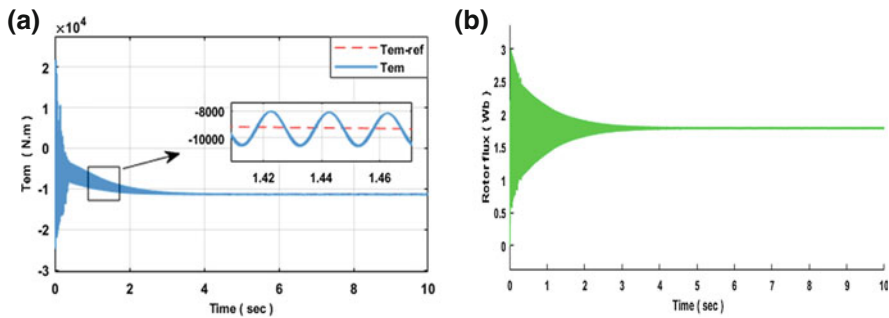


Fig. 8 (a) Electromagnetic torque versus the reference, (b) rotor flux magnitude

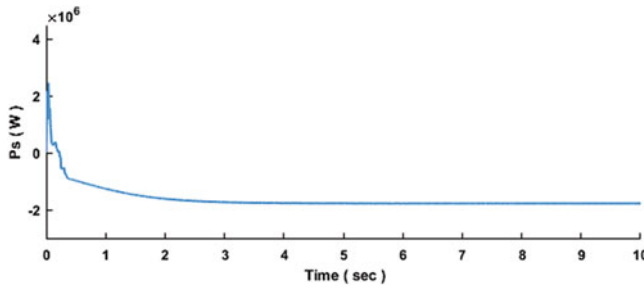


Fig. 9 The stator power

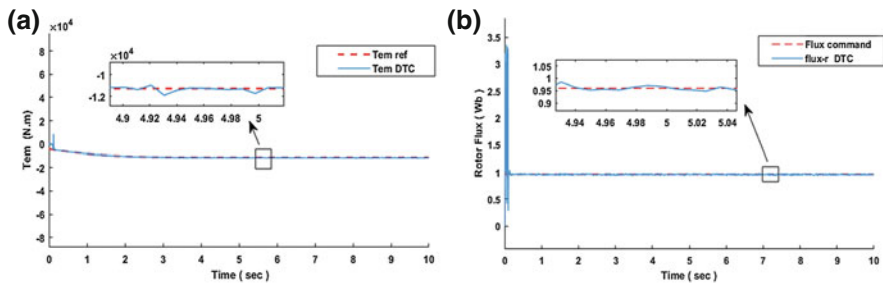


Fig. 10 (a) Electromagnetic torque versus the reference, (b) rotor flux magnitude versus reference

4.2 Direct Torque Control Simulation

In this part, the same parameters of the vector control except the rotor currents will be treated. Besides, the following Fig. 10a, b show the rotor flux amplitude and the electromagnetic torque, starting with rotor flux amplitude which follows the reference ($\psi_r - ref = 0.96 \text{ wb}$) faster as shown in Fig. 10a. Moreover, the Fig. 10b demonstrates how the torque matches the reference rapidly with a neglected error, and both zooms confirm that. Figure 11 displays the stator power delivered to the grid, and we see that after a transient starting, the stator power achieves 1.65 MW at steady state.

4.3 Comparative Studies

In this section, only the electromagnetic torque and the stator power will be compared between both control techniques. The Fig. 12a illustrates the developed electromagnetic torque for the two strategies, and it is clear that the DTC technique coincides with the reference rapidly than the vector control. Besides, the power delivered from the stator for both strategies is shown by Fig. 12b. It is well

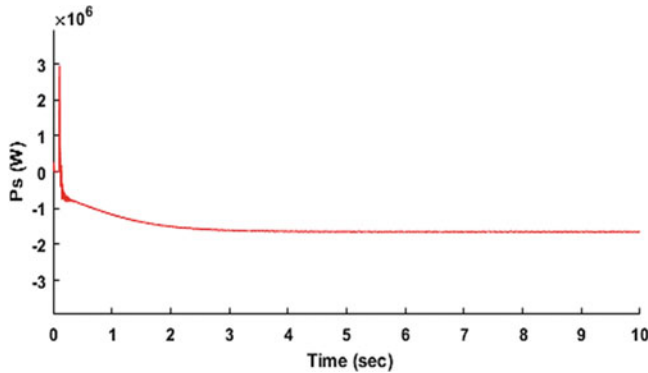


Fig. 11 The stator power

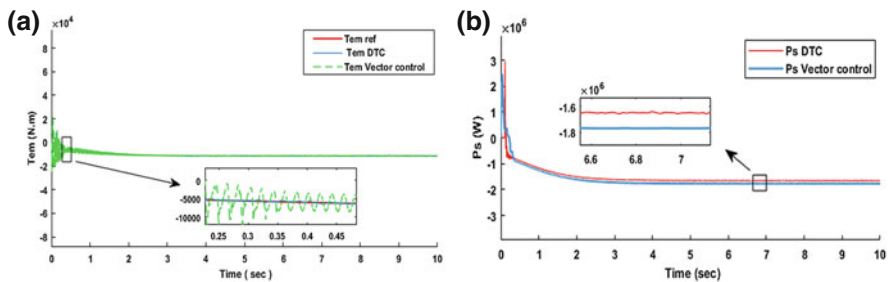


Fig. 12 Comparison of (a) the electromagnetic torque and (b) the stator power

demonstrated that the vector control has more power (1.77 MW) than the DTC (1.65 MW), knowing that in this chapter we use the generator convention, so the negative sign means generating mode.

5 Conclusion

In this chapter, a comparative study between the vector control and the direct torque control (DTC) strategies applied for the rotor side converter (RSC) has been demonstrated. The classic vector control needs many control loops with PI controllers to generate references, but in contrast, it delivered power more than the DTC control. With regard to the DTC, it has a simple configuration and a fast response for both flux and torque, but producing more power losses due to the variable switching frequency. Finally, this study can afford a good support for proper control and operation of the machine in term of performance and complexity of the chosen control techniques.

A.1 Appendix

A.1.1 DFIG-WT Parameters

V_s (line-line) = 690 V, $f = 50$ Hz, $P_{\text{nom}} = 2$ MW, V_r (line-line) = 2070 V, $P = 2$, $u = 1/3$, $I_s = 1070$ A, (max slip) $s_{\text{max}} = 1/3$, (rated) $T_{\text{em}} = 12,732$ N.m, $F_s = 1.9733$ Wb, $R_s = 0.0026$ Ω , $R_r = 0.0029$ Ω , $L_s = L_r = 0.0026$ H, $L_m = 0.0025$ H, $\beta = 0$, $J = 127$ kg m², $f = 0.001$, $\sigma = 0.0661$, $V_{\text{dc}} = 1150$ V, $R = 42$, $\rho = 1.1225$, $G = 100$. $K_{\text{opt}} = 270,000$, $n_s = \text{synchronous speed} = 1500$ rev/min, $s = 0.000002$ s, $V_w = 12$ m/s, (initial slip) = 0.2.

A.1.2 Parameters of the DTC

$T_{s_DTC} = 0.00002$ s

HT = HF = 1%.

A.1.3 Parameters of the PI Controllers

$K_{p_id} = K_{p_iq} = 0.5771$, $K_{i_id} = K_{i_iq} = 491.6$

$K_{p_n} = 10,160$, $K_{i_n} = 406,400$.

References

1. Enerdata. (2018). *The global energy statistical yearbook*. <https://yearbook.enerdata.net>.
2. Dehong, X., Frede, B., Wenjie, C., & Nan, Z. (2018). *Advanced control of doubly fed induction generator for wind power systems*. Wiley.
3. Fox, B., Leslie, B., Damian, F., Nick, J., David, M., Mark, O., Richard, W., & Olimpo, A. (2014). *Wind power integration: Connection and system operational aspects* (2nd ed.). Institution of Engineering and Technology.
4. Kerrouche, K., Mezouar, A., & Belgacem, K. (2013). Decoupled control of doubly fed induction generator by vector control for wind energy conversion system. In *Energy procedia* (pp. 239–248).
5. Fei, G., Tao, Z., & Zengping, W. (2012). Comparative study of direct power control with vector control for rotor side converter of DFIG. In *9th IET International Conference on advances in power system control, operation and management* (pp. 1–6).
6. Arnalte, S., Burgos, J. C., & Rodríguez-Amenedo, J. L. (2013). Direct torque control of a doubly-fed induction generator for variable speed wind turbines. *Electric Power Components & Systems*, 30(2), 199–216.
7. Li, Y., Hang, L., Li, G., Guo, Y., Zou, Y., Chen, J., Li, J., Jian, Z., & Li, S. (2016). An improved DTC controller for DFIG-based wind generation system. In *IEEE 8th International Power Electronics and Motion Control Conference (IPEMC-ECCE Asia)* (pp. 1423–1426).

8. Kumar, A., & GiriBabu, D. (2016). Performance improvement of DFIG fed Wind Energy Conversion system using ANFIS controller. In *2nd International Conference on Advances in Electrical, Electronics, Information, Communication and Bio-Informatics (AEEICB)* (pp. 202–206).
9. Gonzalo, A., Jesus, L., Miguel, R., Luis, M., & Grzegorz, I. (2011). *Doubly fed induction machine modeling and control for wind energy generation*. Wiley.
10. Haitham, A., Mariusz, M., & Kamal, A. (2014). *Power electronics for renewable energy systems, transportation and industrial applications* (1st ed.). Wiley.
11. Zhaoyang, S., Ping, W., & Pengxian, S. (2014). Research on control strategy of DFIG rotor side converter. In *IEEE Conference and Expo Transportation Electrification Asia-Pacific (ITEC Asia-Pacific)* (pp. 1–5).
12. Bin, W., Yongqiang, L., Navid, Z., & Samir, K. (2011). *Power conversion and control of wind energy systems*. Wiley.
13. Zhang, Y., Li, Z., Wang, T., Xu, W., & Zhu, J. (2011). Evaluation of a class of improved DTC method applied in DFIG for wind energy applications. In *International Conference on electrical machines and systems* (pp. 1–6).
14. Jihène, B., Adel, K., & Mohamed, F. M. (2011). DTC, DPC and Nonlinear Vector Control Strategies Applied to the DFIG Operated at Variable Speed. *Journal of Electrical Engineering, 11*(3), 1–13.
15. Xiong, P., & Sun, D. (2016). Backstepping-based DPC strategy of a wind turbine driven DFIG under Normal and harmonic grid voltage. *IEEE Transactions on Power Electronics, 31*(6), 4216–4225.
16. Adel, K., Mohamed, F., & M. (2010). Sensorless-adaptive DTC of double star induction motor. *Energy Conversion and Management, 51*(12), 2878–2892.